Heliyon 7 (2021) e06548

Contents lists available at ScienceDirect

Heliyon

journal homepage: www.cell.com/heliyon

Research article

DFT and molecular dynamics studies of astaxanthin-metal ions (Cu^{2+} and Zn^{2+}) complex to prevent glycated human serum albumin from possible unfolding

Syahputra Wibowo [a], Sri Widyarti [a], Akhmad Sabarudin [b], Djoko Wahono Soeatmadji [c], Sutiman Bambang Sumitro [a,*]

[a] Department of Biology, Faculty of Mathematics and Natural Sciences, Brawijaya University Jl. Veteran, Malang 65145, East Java, Indonesia
[b] Department of Chemistry, Faculty of Mathematics and Natural Sciences, Brawijaya University, Jl. Veteran, Malang 65145, East Java, Indonesia
[c] Department of Internal Medicine, School of Medicine, Brawijaya University, Jl. Veteran, Malang 65145, East Java, Indonesia

ARTICLE INFO

Keywords:
Astaxanthin
Density functional theory
Gaussian 09W
Molecular dynamics simulation
Transition metal ions

ABSTRACT

Glycated human serum albumin (gHSA) undergoes conformational changes of proteins caused by free radicals. The glycation process results in a reduced ability of albumin as an endogenous scavenger in diabetes mellitus type 2 (T2DM) patients. Astaxanthin (ASX) has been shown to prevent gHSA from experiencing unfolding events and improve protein stability of gHSA and HSA through molecular dynamics. In this study, astaxanthin is complexed with transition metal ions such as copper (Cu^{2+}) and zinc (Zn^{2+}) in two modes (M) and (2M). Complexing astaxanthin with Cu^{2+} and Zn^{2+} is expected to increase astaxanthin's ability as an endogenous scavenger than in native form. This research aims to characterize the antiradical property of ASX, ASX-Cu^{2+} and ASX-2Cu^{2+}, ASX-Zn^{2+}, and ASX-2Zn^{2+} with density functional theory (DFT) and to compare the capability to prevent conformational changes on glycated albumin through molecular dynamics simulation. DFT as implemented in Gaussian 09W, was used for all calculations. Analysis of data using GaussView 6.0. LANL2D2Z basis set and B3LYP density functional used for frequency analysis and optimization. The AutoDock Vina implemented in PyRx 0.8 is used to and receptor-ligand interactions analysis with the DS 2016 Client. YASARA for molecular dynamic simulation with 15,000 ps as running time. DFT analyzes such as energy gaps, HOMO, and LUMO patterns and electronic properties have shown that ASX-metal ions complex is better than ASX in native state as antioxidants. These results are also supported by the molecular dynamics simulation (RMSD backbone, RMSDr, RMSFr, and movie visualization), where the addition of ASX-metal ions complex on gHSA are better than ASX as a single compound in preventing gHSA from possible unfolding and maintaining protein molecule stability.

1. Introduction

The presence of oxidative stress in the cellular system induces numerous human health problems [1]. Free radicals that surpass the defensive potential of cells in the human body will induce oxidative stress [2]. One of the oxidative damages caused by free radicals is a modification in albumin protein conformation in diabetes mellitus type 2 (T2DM) patients [3]. Albumin is a protein that is directly affected by the increase in free radicals in the blood. This condition disrupts albumin function as both a scavenger and a transporter [4].

Albumin's ability as a scavenger is one of them is metal ions binding were as previously known that heme has pro-oxidant properties, and albumin is an adequate protein in heme binding. When bonded with albumin, the pro-oxidant properties of heme experience a decrease that identifies albumin as having a function as an antioxidant [5]. Albumin is also proven to bind various kinds of metal ions such as Cu^{2+}, Fe^{2+}, Mn^{2+}, Mn^{3+}, and Fe^{3+} with active residues such as Cys34 [6]. The redox status of the thiol group in the protein is a crucial indicator of oxidative stress so that the measurement of Cys-34 redox in human albumin serum can determine organ damage. From the results of ESI-TOFMS, it was found that the highest form of oxidation is found in Cys-34. Oxidative stress results in modifications of residues Lys195, Lys190, Arg218, Trp211, and Arg222 that function as ligand bindings for site one and Arg410 as

* Corresponding author.
E-mail address: sutiman@ub.ac.id (S.B. Sumitro).

https://doi.org/10.1016/j.heliyon.2021.e06548
Received 1 December 2020; Received in revised form 2 February 2021; Accepted 11 March 2021

Tyr411 in site two. It was found that 80% of the –SH cluster that is a potent ROS scavenger in albumin comes from Cys-34 [7].

The presence of cysteine and methionine residues is significant in HSA antioxidant abilities. When mutations are carried out on Cys34, albumin's antioxidant ability drops by 30%, and if the free cysteine residue is placed in another position on the HSA, it still has antioxidant capabilities. Site 2 of the HSA is the target of oxidative stress, but lost or modified cysteine residues result in albumin proteins being more easily degraded [8]. Albumin protein damage, including unfolding events, has been reviewed in our previous studies using molecular dynamics (MD) analysis, in which human serum albumin (HSA) and glycated human serum albumin (gHSA) were tested for 15,000 ps and showed that the unfolding process in gHSA caused the breakup of side chains A and B in those proteins [9]. Antioxidants are needed by the body of T2DM sufferers to overcome unfolding events and maintain the stability of proteins affected by free radicals [10]. Antioxidants have an essential role in balancing electrons in oxidative stress conditions, one of which comes from the carotene group. This is because antioxidants can act as donors as well as electron acceptance [11]. One of the carotene group's antioxidants that has a high potential as an antioxidant is astaxanthin (ASX) [12], as one of the lipophilic compounds terpene astaxanthin has a polyene chain that has the ability the stabilization free radicals [13]. As a radical scavenger, astaxanthin has several action mechanisms, namely hydrogen atom transfer, radical adduct, and single electron transfer [14]. Our previous research has shown that ASX administration in gHSA and HSA can maintain the protein conformation until the end of the molecular dynamics simulation. The conclusion is supported by backbone RMSD, RMSF, and movie visualization data [9].

In this study, astaxanthin will be complexed with several metal ions and configurations, namely Cu^{2+} and Zn^{2+}. The selection of these two transition metal ions due to the transition metal ions that are central to the biological complex mainly has the principle of redox and Lewis acid. Redox activities such as shuttle electron can be done by transition metal ions that are already bonded with specific proteins [15]. Analysis using density functional theory (DFT) and molecular dynamics for ASX in a complex form with metal ions and interacted with gHSA has never been done before. The purpose of this research is to understand at increased capabilities of ASX, which has been complexed with metal ions as antioxidants in the role of maintaining gHSA stability compared to the ASX in native form.

2. Materials and methods

This research does not have any IACUC/IRB approval because there was no human, animal, or cell involvement. This research was purely in silico studies.

2.1. Materials

Data mining has been carried out from PubChem (http://www.pubchem.ncbi.nlm.nih.gov) and PDB (http://www.rscb.org/pdb) databases to obtain the required data. The compounds used are ASX (5281224), glucose (79025), Cu^{2+} (27099) and Zn^{2+} (32051). Meanwhile, the protein used is HSA with PDB ID (4K2C).

2.2. Density functional theory (DFT)

The ASX-metal ions complex is made in Avogadro software by inputting the SMILES isomeric from ASX. The ASX-metal ions complex is divided into two for each type of metal ion complexed with ASX, namely the ASX-M^{2+} and ASX-$2M^{2+}$ configurations. Furthermore, we have optimized the geometry with a setup force field (UFF), the number of steps (500), and an algorithm (Steepest Descent). After the complex was formed, the DFT [16,17,18] software Gaussian09 and GaussView 6.0 were used for all calculations [19]. The method used is Ground State with LANL2DZ basis set [20,21,22,23] and B3LYP density functional [24,25,26] used for frequency analysis and optimization. The LANL2DZ basis set was chosen because it meets DFT calculation requirements on the interaction of metal ions such as cadmium and zinc [27,28,29,30,31,32].

2.3. Molecular docking

The preparation of ASX and ASX-metal ions compounds has been carried out in the Open Babel program by changing the format (.sdf) to (.pdbqt) then HSA protein is cleaned from ligand and water with Discovery Studio 2016 Client and saved in (.pdb) format. The docking process uses AutoDock Vina, which is included in the PyRx 0.8 software. Vina search box applies to all docking processes with dimensions (Å): X (90.1439), Y (109.1736), and Z (79.3440), while the center of box uses X (11.5350), Y (-23.336), and Z (5.6978).

2.4. Molecular dynamics simulation

YASARA has been used to run molecular dynamics simulations [33] for 15,000 ps with physiological pH configurations at 7.4 and 0.9% NaCl for ion concentration as a mass fraction. The temperature used is 310K, and water as solvent with a density of 0.997 g/l. RMSD (root mean square deviation), RMSF (root mean square fluctuation), potential and binding energy, also movie visualization were obtained from this MD simulation.

3. Results and discussion

3.1. DFT analysis

Astaxanthin (3,3′-dihydroxy-β-β-carotene-4,4′-dione) as a ketocarotenoid [34] has the molecular formula C40H52O4 with a molar mass of 596.84 g/mol. Two terminal rings connected by a polyene chain of either single or double bonds are characteristic of this compound. Astaxanthin can be found in several forms, such as the stereoisomeric form, geometric isomer, free form, and esterified form (both hydroxyl groups react with fatty acids). Astaxanthin has two asymmetric carbon atoms in the 3,3′position of the β-ionone ring with a hydroxyl (-OH) functional group at both ends of the molecule. All of these forms are found in natural sources, with the stereoisomeric forms (3S, 3′S) and (3R, 3′R) being the most common in nature [35]. Unlike other carotene compounds, the ring structure of Astaxanthin is each oxygenated with polyene chains double-bound as a backbone as well, thus enhancing the antioxidant properties of Astaxanthin [14].

In this research, ASX is complexed with two transition metal atoms, namely Cu^{2+} and Zn^{2+}, in two-mode configurations, namely one metal (M) and two metals (2M). Figure 1 shows that both Cu^{2+} and Zn^{2+} (M) and (2M) metal ions, when complexed with astaxanthin and performed geometry optimization, resulted in a change in the ASX structure from *trans* to *cis*. This change from *trans* to *cis* is very reasonable because astaxanthin is easily isomerized when exposed to heat, acid, metal ions, or light [36]. Changes in astaxanthin's geometric structure when complexed with transition metal ions to *cis* increase astaxanthin's ability as an antioxidant. *Cis* astaxanthin such as 9-*cis* and 13-*cis* astaxanthin has been shown to have higher antioxidants than its natural form [37]. It even has a bioaccessibility level and is more efficiently absorbed by Caco-2 cells in the human intestine [38].

Charge distribution was studied by using FMO (frontier molecular orbital theory) in this experiment. HOMO (Highest Occupied Molecular Orbital) and LUMO (Lowest Unoccupied Molecular Orbital) energies and energy gap were calculated [39] for understanding the stability of ASX in native and complex forms. Table 1 indicates that the ASX, which is complexed with Zn^{2+} transition metal ions, has the least energy gap compared to the ASX complex with both Cu^{2+} and native ASX. This energy gap means the ASX-Zn^{2+} and ASX-$2Zn^{2+}$ complexes have higher antioxidant activity than ASX compounds in complex form with both Cu^{2+} and native. The structure with lower HOMO energy is a weak electron donor [39], so it can be concluded that the scavenging activity

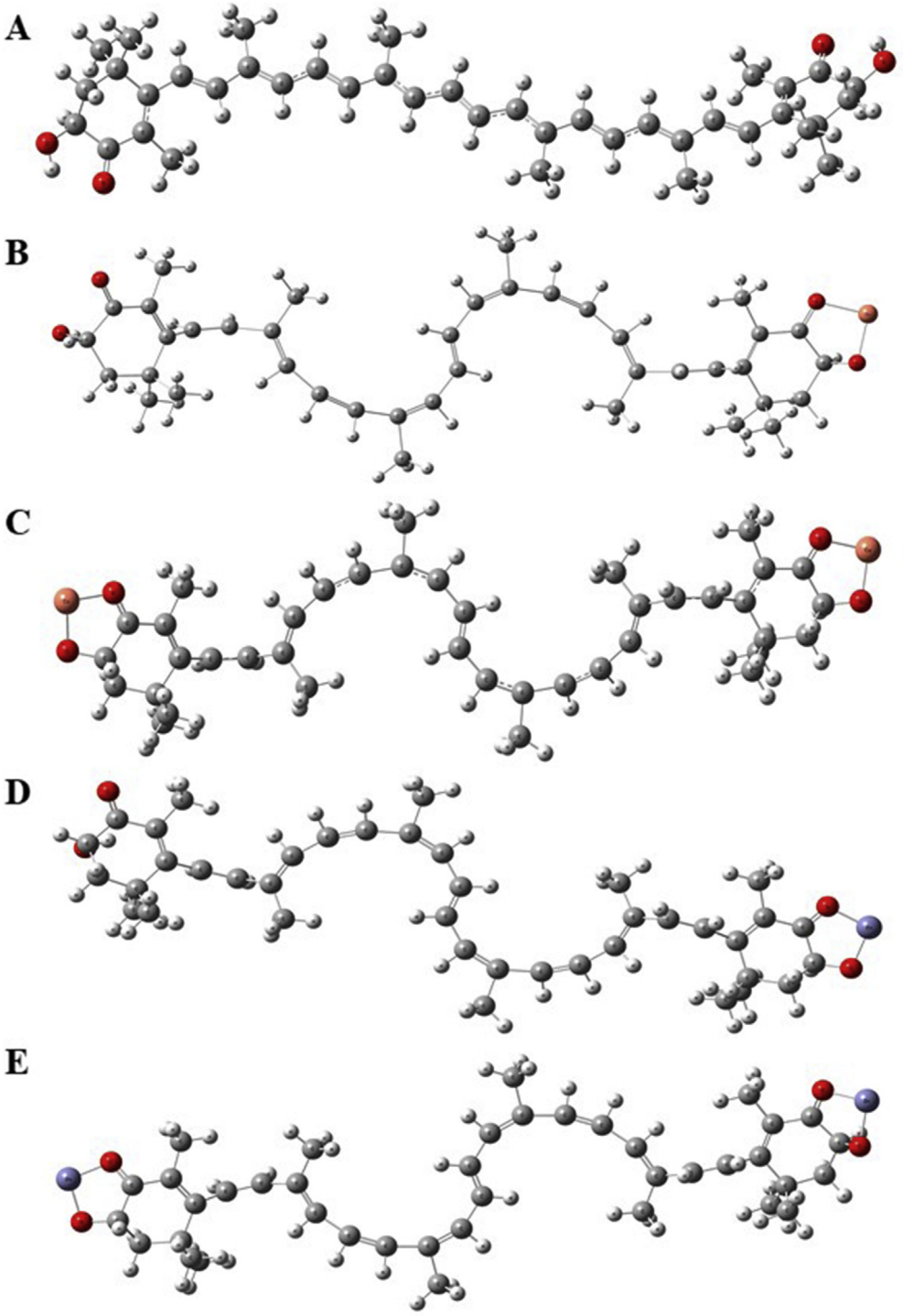

Figure 1. Optimized structures of (A) ASX in native form (B) ASX-Cu^{2+} (M) (C) ASX-$2Cu^{2+}$ (2M) (D) ASX-Zn^{2+} (M) (E) ASX-$2Zn^{2+}$ (2M).

Table 1. HOMO and LUMO.

Compound	HOMO (eV)	LUMO (eV)	Energy Gap
ASX	-5.032	-2.545	2.487
ASX-Cu^{2+}(M)	-5.257	-2.506	2.752
ASX-$2Cu^{2+}$(2M)	-5.275	-2.495	2.780
ASX-Zn^{2+}(M)	-2.863	-2.498	0.365
ASX-$2Zn^{2+}$(2M)	-2.445	-2.234	0.211

sequence from low to highest is **ASX-2Cu^{2+}(2M) < ASX-Cu^{2+}(M) < ASX < ASX-Zn^{2+}(M) < ASX-2Zn^{2+}(2M)**.

Figure 2 shows that there is a variation in the pattern of HOMO and LUMO from ASX in the original and complex form. Excited-state on the ASX native from 162 (HOMO) to 163 (LUMO), then to ASX-Cu^{2+}(M) from 171 to 172. While the ASX-2Cu^{2+}(2M) has an excited state from 180 to 181, meanwhile ASX-Zn^{2+}(M) from 168 to 169 and ASX-2Zn^{2+}(2M) from 173 to 174. The green color in Figure 2 indicates a positive charge when the negative charge is red. Overlapping conditions that emerge in native ASX (Figure 2A.) shows that electrons will excite easily but have difficulty in the reverse process, which is less efficient as an antioxidant when expected to have the ability to reverse quickly so that the products resulting from scavenging activity can be more. From Figure 2 it can be concluded that the addition of transition metal ions makes ASX a better antioxidant than ASX in the native state. Similar results were also shown by Marin et al. [40], where the formation of the ASX-metal cationic complex had slightly better as electron donors and acceptors compared to single ASX. The consequence of increasing the electron transfer capacity has a positive correlation with the increase in the ability of ASX as a free radical scavenger.

The data in Figure 3 were obtained by a method using a polarizable continuum model, particularly IEF-PCM (integral-equation-formalism) with ethanol as a solvent, to resolve the situation in the laboratory. The formation of the ASX complex with transition metal ions has a negative overall energy value, meaning that the reaction products are more stable than the reactants (Figure 3A.) [40]. In contrast, ASX's thermal energy in native form has higher energy than in complex forms but has the lowest dipole moment compared to ASX in complex forms. Thermodynamically, ASX in *trans* form more stable than the *cis* form, but from the energy gap and the dipole moment, it can be concluded that the ASX structure in the native state that is stable does not have better scavenging electrons than in the complex form with transition metal ions. Next is heat capacity (Figure 3D.), which is the amount of heat needed to raise the temperature of one kilogram (kg) of mass by one kelvin (K), showing that ASX-metal ions have a higher value compared to ASX in a native state.

3.2. Molecular docking analysis

To understand the ability of ASX-metal ions complex compared to ASX in the native state towards gHSA, the first thing to do is molecular docking. To get GHSA, HSA is complexed with glucose first (Figure 4A), where the binding affinity is -5.8 kcal/mol. As the ASX, which is paired with gHSA, has a binding affinity of -8.9 kcal/mol, the binding affinity value is the energy required of a compound to interact with the target protein. The lower the energy needed, the stronger and more manageable the bond between ligands and proteins is. In our previous study [9], ASX complexed with normal HSA has a bond at site A, and in this study, it was found that ASX is a smart ligand since the binding position is at site B, the site where glycation in gHSA occurs. Likewise with ASX, which is complexed with both Cu^{2+} and Zn^{2+} metal ions in (M) and (2M) modes. ASX-metal ion complexes bind more easily to the target protein because they have a lower binding affinity than ASX in native form.

The binding site analysis (Figure 5) showed that unfavorable donors occurred in the interaction between glucose and human serum albumin. Meanwhile, the protein residues in the docking results of ASX and gHSA have pi-alkyl, alkyl, and hydrogen bond types. The same type of bonding pattern is also seen in the ASX-metal ions, which bind to gHSA. The difference occurs in the number of types of pi-alkyl bonds that have increased in (gHSA-(ASX-2Cu^{2+})) (gHSA- (ASX-Zn^{2+})) and (gHSA-(ASX-2Zn^{2+})) complex.

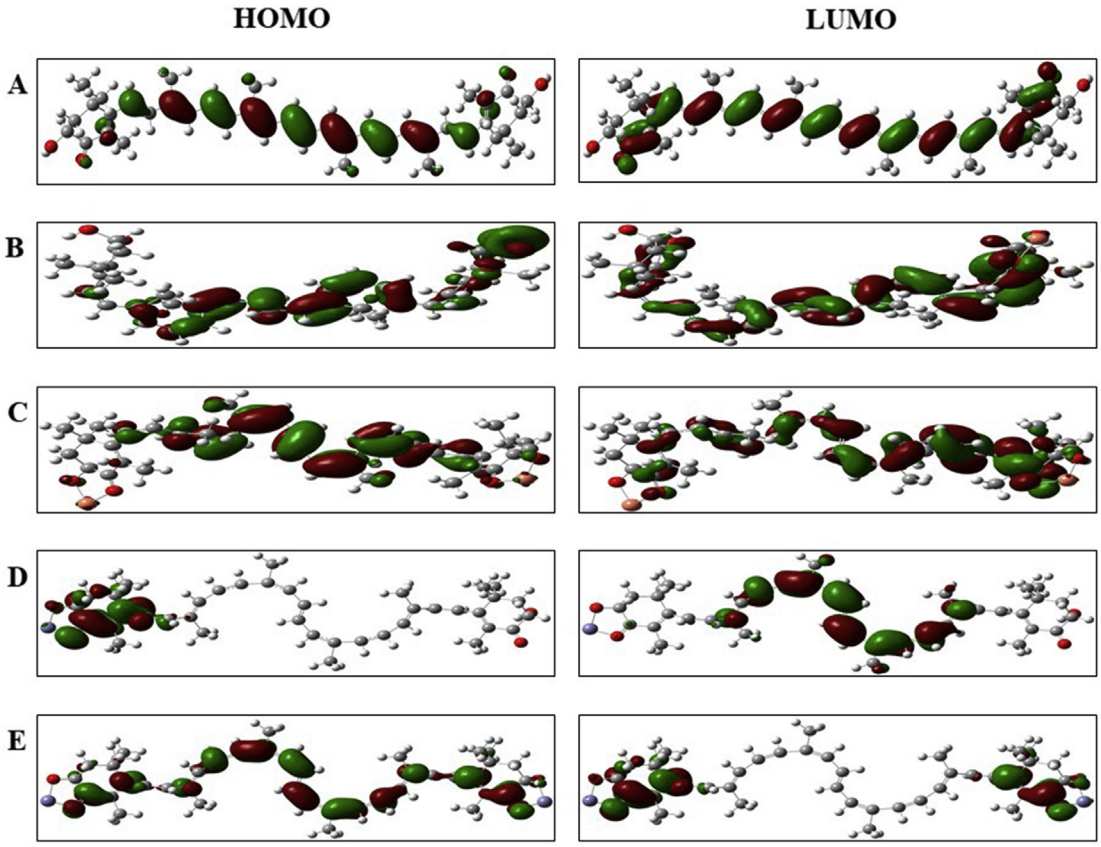

Figure 2. HOMO and LUMO of (A) ASX in native form (B) ASX-Cu^{2+} (M) (C) ASX-2Cu^{2+} (2M) (D) ASX-Zn^{2+} (M) (E) ASX-2Zn^{2+} (2M).

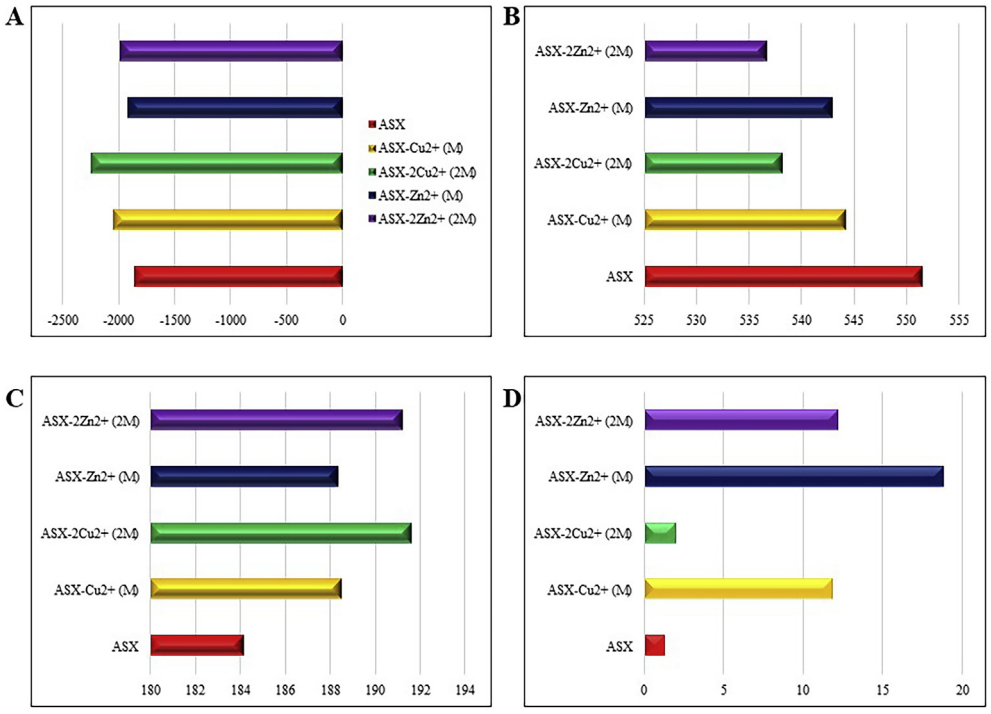

Figure 3. Data compilation of (A) Total Energy (Hartree) (B) Thermal Energy (kcal/mol) (C) Heat Capacity (cal/mol K) (D) Dipole Moment (Debye).

3.3. Molecular dynamics analysis

The potential and binding energy (Figure 6) have shown that both ligand and protein complexes have been reached an equilibrium state so that the data obtained are reliable. In the case of potential energy, the initial state value is obtained from HSA, gHSA, gHSA-ASX, gHSA-(ASX-Cu^{2+}), gHSA-(ASX-$2Cu^{2+}$), gHSA-(ASX-Zn^{2+}), gHSA-(ASX-$2Zn^{2+}$) are -2276091.99 kJ/mol, -2273555.43 kJ/mol, -2262791.79 kJ/mol, -2258417.372 kJ/mol, -2278815.281 kJ/mol, -2275741.254 kJ/mol, and -2277063.146 kJ/mol, respectively. In the meantime, binding energy has an initial state value of HSA, gHSA, gHSA-ASX, gHSA-(ASX-Cu^{2+}), gHSA-(ASX-$2Cu^{2+}$), gHSA-(ASX-Zn^{2+}), gHSA-(ASX-$2Zn^{2+}$) are 97982.87 kJ/mol, 98017.75 kJ/mol, 97102.55 kJ/mol, 130080.48 kJ/mol, 98016.05 kJ/mol, 98026.296 kJ/mol and 97925.865 kJ/mol, respectively. The equilibrium state starts at 300 ps for both potential energy and binding energy. In (Figure 7) it can be shown that the addition of ASX to gHSA (black color) can consistently reduce the RMSD backbone of gHSA until the end of the simulation. In the meantime, gHSA encountered an unfolding event because the RMSD value was more than 4 nm at 2300 ps, to be precise 4.343 nm, while the standard HSA at the same time had an RMSD value of 2.834 nm, and the addition of ASX to the gHSA protein lowered the RMSD backbone to 4.176 nm. The addition of transition metal ions such as Cu^{2+} and Zn^{2+} in both (M) and (2M) ASX modes was able to reduce the RMSD backbone of gHSA to close to normal HSA values, with gHSA-(ASX-Cu^{2+}), gHSA-(ASX-$2Cu^{2+}$), gHSA-(ASX-Zn^{2+}), gHSA-(ASX-$2Zn^{2+}$) having values of 2.827 nm, 2.946 nm, 2.794 nm and 3.263 nm respectively. The RMSD backbone value at the end of the molecular dynamics simulation at 15,000 ps shows that gHSA is 9.052 nm compared to HSA of 7.561 nm.

While the gHSA-ASX complex reached 5,028 nm and the ASX-metal ion complex included gHSA-(ASX-Cu^{2+}), gHSA-(ASX-$2Cu^{2+}$), gHSA-(ASX-Zn^{2+}), gHSA-(ASX-$2Zn^{2+}$) had a lower value than ASX in the native state to gHSA of 4.874 nm, 3.895 nm, 4.346 nm and 4.929 nm respectively. This suggests an improvement in ASX's potential as a scavenger in a complex form with transition metal ions compared to ASX in the native state. It can also be concluded that the DFT results are in line with the results of molecular dynamics simulation.

More complex analyzes were also carried out, including RMSDr (Figure 8) and RMSFr (Figure 9). The residues selected in (Figure 8) and (Figure 9) are binding sites of ligands to gHSA and compared RMSDr and RMSFr of each active residue both before and after administration ASX and ASX-metal ions. Figure 8A reaffirming the previous RMSD backbone data that at the end of the simulation at 15,000 ps, the residue where the glycation occurs has an increase in RMSD, which causes unfolding and destabilization of protein events. The residue SER193 (B), GLN459 (B), ARG145 (B), and ASP108 (B) are the sites of the glycation process in HSA. When compared, the data show that at gHSA, the residual RMSD values of SER193 (B), GLN459 (B), ARG145 (B), and ASP108 (B) were 4.316 nm, 4.747 nm, 2.829 nm, and 3.635 nm, respectively. Whereas for HSA, the residual RMSD values for SER193 (B), GLN459 (B), ARG145 (B), and ASP108 (B) were 1.872 nm, 3.25 nm, 2.618 nm, and 2.845 nm, respectively. There was also an RMSDr comparison of gHSA and ASX-gHSA complexes (Figure 8B) where the RMSD value of each gHSA protein amino acid residue given by ASX decreased when compared to those without ASX. These data confirm the RMSD backbone findings as a whole to make the gHSA protein more stable when administered by ASX. Examples are the residual PHE228 (B) in gHSA has an RMSDr of 8.446 nm, which decreases to 4.445 nm when complexed with ASX and the VAL216 (B) residue from 6.847 nm to 3.981 nm. Meanwhile, compared to the ASX complexed with Cu2+ ion in (M) mode, the residual PHE228 (B) has a value of 3.089 nm and an RMSDr of 2.201 nm in mode (2M). The VAL216 (B) residue in the gHSA-(ASX-Cu^{2+}) complex was 2.818 nm and the gHSA-(ASX-$2Cu^{2+}$) was 1.982 nm. The same thing also happened with gHSA-(ASX-Zn^{2+}) and gHSA-(ASX-$2Zn^{2+}$) complexes with the same residues, which have lower RMSDr than gHSA without ASX or when complexed with ASX in the native state. This decrease in the value of RMSDr induced the gHSA protein that had previously undergone unfolding and binding sites release of side chains A and B became very stable until the end of the molecular dynamics simulation.

The RMSFr data (Figure 9) show the same pattern as the RMSDr. Residues such as VAL325(B) in gHSA have a value of 4.192 nm and when given ASX it becomes 2.576 nm, whereas in the gHSA-(ASX-Cu^{2+}), gHSA-(ASX-$2Cu^{2+}$), gHSA-(ASX-Zn^{2+}) and gHSA-(ASX-$2Zn^{2+}$) complexes are 3.19 nm, 2.349 nm, 2.835 nm, 2.297 nm respectively. Meanwhile, the

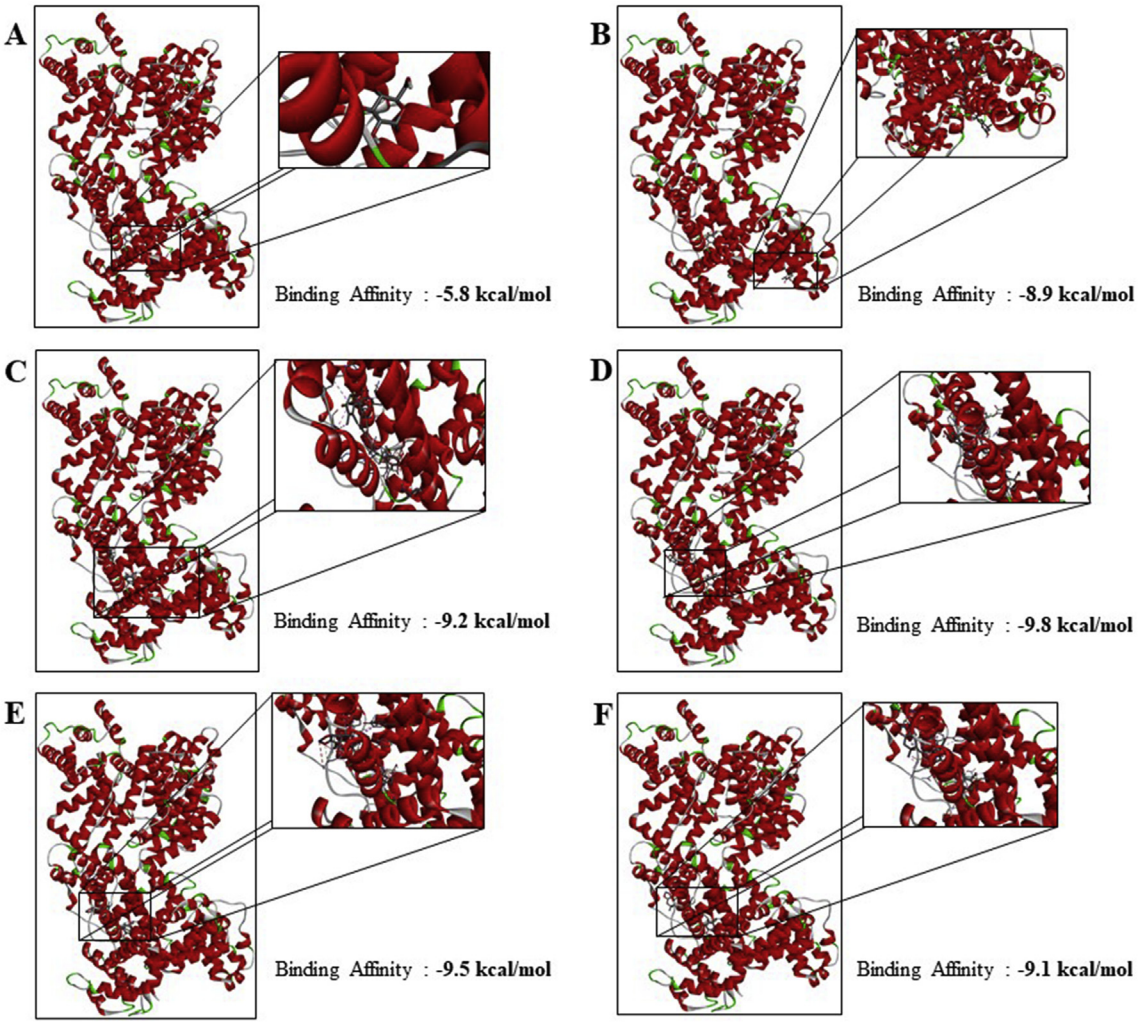

Figure 4. Docking result (A) gHSA (B) gHSA-ASX (C) gHSA-(ASX-Cu^{2+}) (D) gHSA-(ASX-$2Cu^{2+}$) (E) gHSA-(ASX-Zn^{2+}) (F) gHSA-(ASX-$2Zn^{2+}$).

LEU 327 (B) residue in gHSA was 4.104 nm, while gHSA-ASX became 2.545 nm. When ASX is complex with metal ions such as gHSA-(ASX-Cu^{2+}), gHSA-(ASX-$2Cu^{2+}$), gHSA-(ASX-Zn^{2+}) and gHSA-(ASX-$2Zn^{2+}$), the RMSFr value of residual LEU327 (B) becomes 3.157 nm, 2.171 nm, 2.684 nm and 1.921 nm respectively. Other residues such as ALA350 (B) in ghSA have an RMSFr value of 3.703 nm, while the addition of ASX reduces the value to 2.087 nm. The addition of ASX-metal ions ((gHSA-(ASX-Cu^{2+}), gHSA-(ASX-$2Cu^{2+}$), gHSA-(ASX-Zn^{2+}) and gHSA-(ASX-$2Zn^{2+}$)) to gHSA system makes RMSFr from residual ALA350 (B) to 2.58 nm, 1.95 nm, 2.35 nm and 1,725 nm, respectively.

gHSA	gHSA-ASX	gHSA-(ASX-Cu^{2+})	gHSA-(ASX-$2Cu^{2+}$)	gHSA-(ASX-Zn^{2+})	gHSA-(ASX-$2Zn^{2+}$)
SER193(B)	VAL325(B)	TYR161(B)	ASP183(B)	LYS137(B)	ASP108(B)
GLN159(B)	PHE228(B)	ILE142(B)	ILE142(B)	PHE134(B)	SER193(B)
ARG145(B)	VAL482(B)	ARG145(B)	LEU115(B)	ARG186(B)	ARG145(B)
ASP108(B)	LYS351(B)	LEU115(B)	LYS137(B)	LEU115(B)	VAL122(B)
	ARG348(B)	ARG117(B)	PRO118(B)	MET123(B)	ALA126(B)
	LEU380(B)	ARG186(B)	MET123(B)	ARG114(B)	ALA194(B)
	ALA350(B)	ILE523(B)	ARG145(B)	LEU463(B)	PRO118(B)
	LEU327(B)	VAL462(B)	ILE523(B)	VAL462(B)	MET123(B)
	ALA213(B)	LEU463(B)	LYS519(B)	TYR138(B)	LYS137(B)
	VAL216(B)	HIS146(B)	ARG186(B)	HIS146(B)	ARG114(B)
	LEU331(B)		PHE134(B)	TYR161(B)	LEU463(B)
	ARG209(B)		TYR138(B)		PHE134(B)
	LYS212(B)		HIS146(B)		HIS146(B)
					TYR161(B)

Hydrogen Bond
Unfavorable Donor-Donor
Alkyl Bond
Pi-Alkyl Bond

Figure 5. Interaction residues of docking.

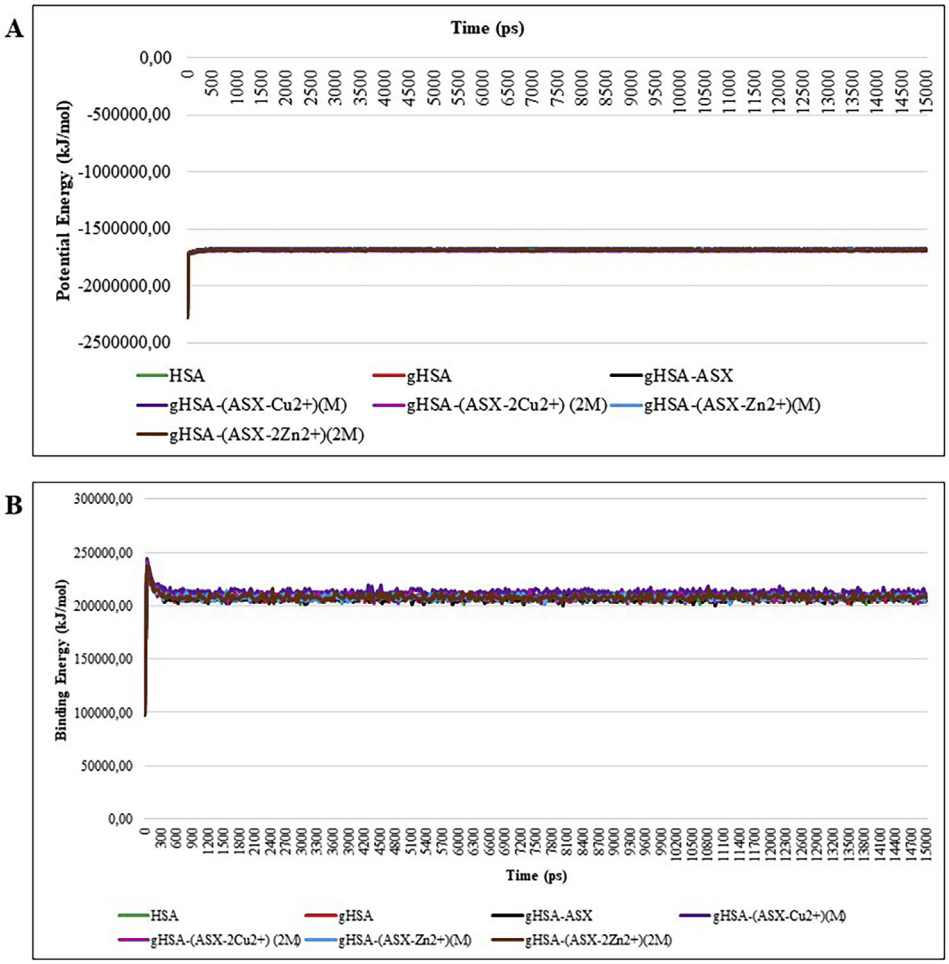

Figure 6. Molecular dynamics data (A) potential energy (B) binding energy.

Movie visualization data (Figure 10) has been obtained from macro analysis (md_play) in the YASARA app. Movie visualization data is visual data from RMSD, RMSDr, and RMSFr. Figure 9 is a visualization of HSA, gHSA, gHSA-ASX, gHSA-(ASX-Cu^{2+}), gHSA-(ASX-$2Cu^{2+}$), gHSA-(ASX-Zn^{2+}) and gHSA-(ASX-$2Zn^{2+}$) in the final state of molecular dynamics simulation at 15,000 ps. Side chain A of HSA or gHSA was colored in blue and green for side chain B. As shown in Figure 9B gHSA undergoes an unfolding process and releases the bonds between its amino acid residues, especially in the protein linker area between side A and B. While giving ASX makes gHSA, which was previously unstable and unfolding back to stability and approaching the conditions before the glycation process occurred. The ASX complex with metal ions proved to be better than the ASX as a single compound in preventing the unfolding process on the gHSA protein. For Cu^{2+} transition metal ions with gHSA-(ASX-$2Cu^{2+}$) (2M) configuration slightly better than gHSA-(ASX-Cu^{2+}) (M). As for the ASX complex with Zn^{2+} ions, the gHSA-(ASX-$2Zn^{2+}$) (2M) configuration is better than gHSA-(ASX-Zn^{2+}) (M). It is based on RMSD

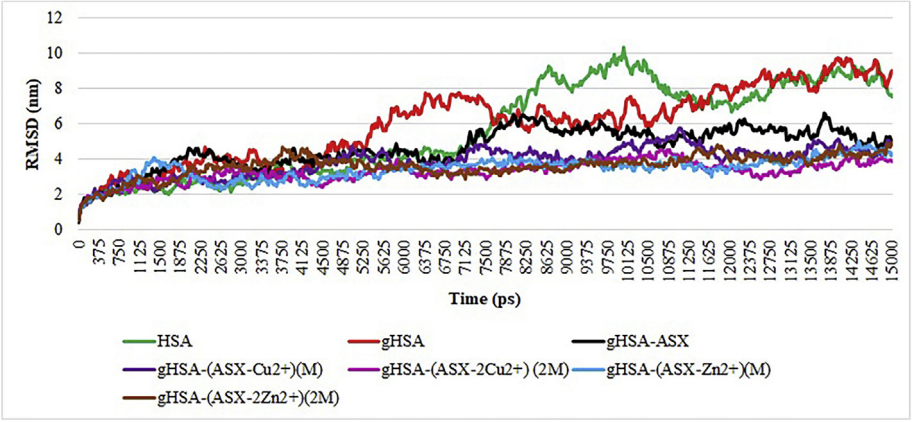

Figure 7. RMSD backbone.

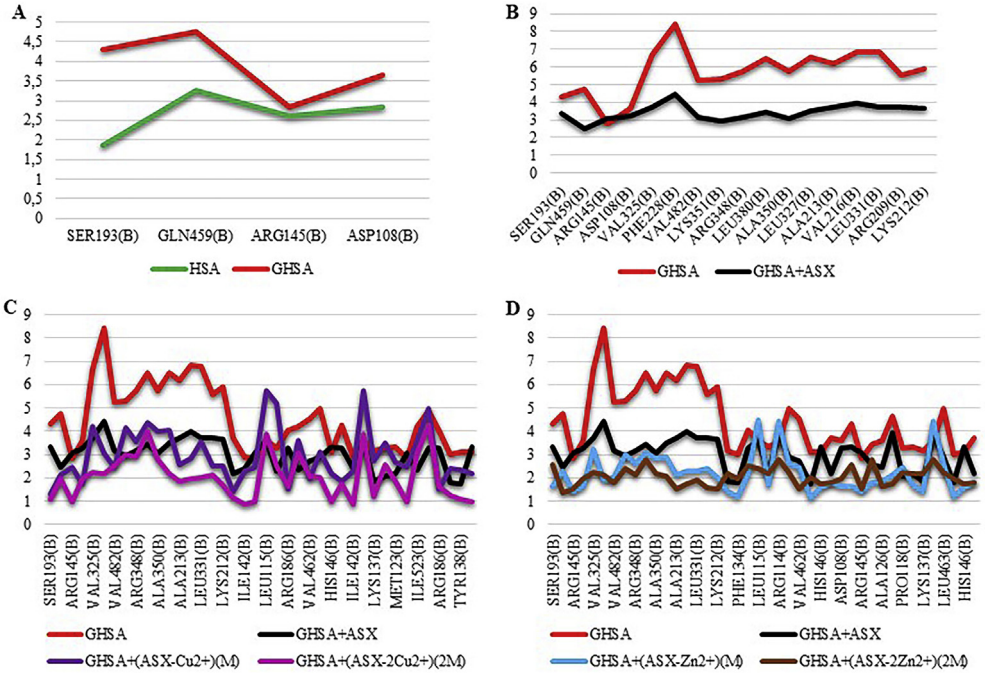

Figure 8. RMSDr of (A) HSA and gHSA (B) gHSA and gHSA-ASX (C) gHSA, gHSA-ASX, gHSA-(ASX-Cu^{2+}) and gHSA-(ASX-$2Cu^{2+}$) (D) gHSA, gHSA-ASX, gHSA-(ASX-Zn^{2+}) and gHSA-(ASX-$2Zn^{2+}$).

backbone data, RMSDr, RMSFr, and movie visualization. Research conducted by Marin et al. [40] supports the results of data from this study that ASX-metal cationic system has better electron donators compared to ASX because there was a decrease of vertical ionization energy and increment of vertical electron affinity that implies metallic complexes are better electron acceptor than ASX in the native state.

4. Conclusion

Astaxanthin as an antioxidant has been shown to prevent damage to albumin glycated human serum proteins such as unfolding and modification of active sites that cause the release of binding sites on side chains A and B. DFT analyses such as energy gaps, HOMO, and LUMO patterns as well as electronic properties have shown that ASX-metal ions complex is

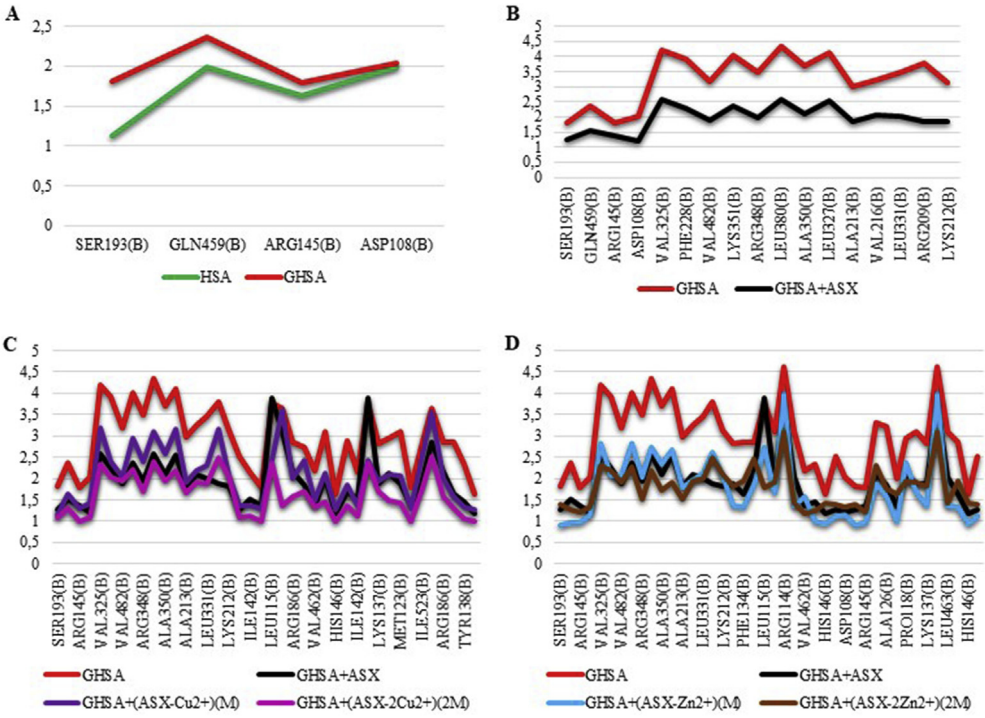

Figure 9. RMSFr of (A) HSA and gHSA (B) gHSA and gHSA-ASX (C) gHSA, gHSA-ASX, gHSA-(ASX-Cu^{2+}) and gHSA-(ASX-$2Cu^{2+}$) (D) gHSA, gHSA-ASX, gHSA-(ASX-Zn^{2+}) and gHSA-(ASX-$2Zn^{2+}$).

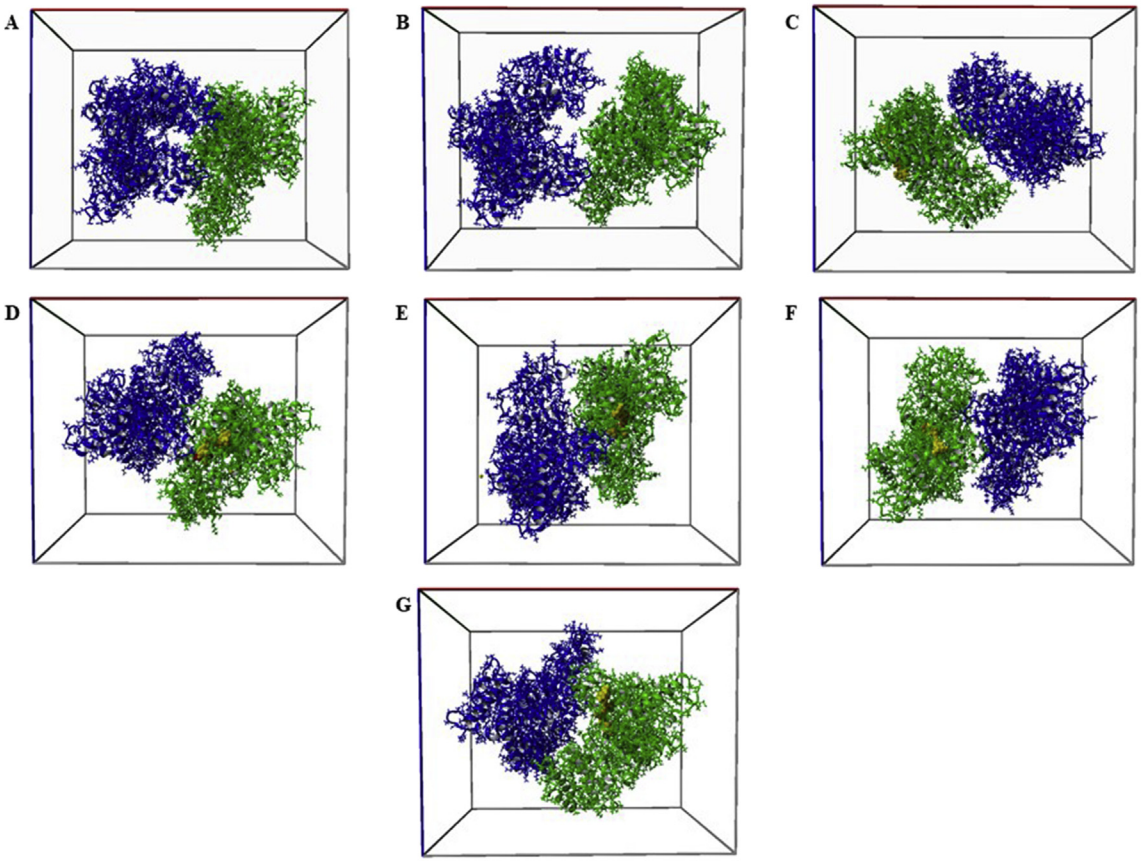

Figure 10. Movie visualization of (A) HSA (B) gHSA (C) gHSA-ASX (D) gHSA-(ASX-Cu^{2+}) (E) gHSA-(ASX-$2Cu^{2+}$) (F) gHSA-(ASX-Zn^{2+}) (G) gHSA-(ASX-$2Zn^{2+}$). Side chain A (blue) and side chain B (green) identified by YASARA.

better than ASX in native state as antioxidants. This is supported by data from molecular dynamics simulation consisting of RMSD backbone, RMSDr, and RMSFr data as well as movie visualization that provides information that ASX-metal ions complex, especially ASX-$2Cu^{2+}$ and ASX-$2Zn^{2+}$, are better than ASX as a single compound in preventing gHSA damage and maintaining protein molecule stability until the end of molecular dynamics simulation at 15,000 ps.

Declarations

Author contribution statement

Syahputra Wibowo: Conceived and designed the experiments; Performed the experiments; Analyzed and interpreted the data; Contributed reagents, materials, analysis tools or data; Wrote the paper.

Akhmad Sabarudin, Sri Widyarti, Djoko Wahono Soeatmadji, Sutiman Bambang Sumitro: Conceived and designed the experiments; Analyzed and interpreted the data.

Funding statement

This work was supported by the Ministry of Research, Technology and Higher Education of Indonesia through the scheme of PMDSU.

Data availability statement

Data will be made available on request.

Declaration of interests statement

The authors declare no conflict of interest.

Additional information

No additional information is available for this paper.

References

[1] G. Pizzino, N. Irrera, M. Cucinotta, G. Pallio, F. Mannino, V. Arcoraci, A. Bitto, Oxidative stress: harms and benefits for human health, Oxid Med Cell Longev (2017) 8416763.

[2] N.E. Polyakov, A.L. Focsan, M.K. Bowman, L.D. Kispert, Free radical formation in novel karotenoid metal in complexes of astaxanthin, J. Phys. Chem. B 114 (50) (2010) 16968–16977.

[3] R.K. Murray, D.K. Granner, P.A. Mayes, V.W. Rodwell, Harper's Illustrated Biochemistry, 26th ed., Mcgraw Hills Companies, Boston, 2003.

[4] M. Fasano, S. Curry, E. Terreno, M. Gilliano, G. Fanali, P. Narciso, S. Notari, P. Ascenzi, The extraordinary ligand binding properties of human serum albumin, IUBMB Life 57 (12) (2005) 787–796.

[5] G.J. Quinlan, G.S. Martin, T.W. Evans, Albumin : biochemical and therapeutic potential, Hepatology 41 (6) (2005) 1211–1219.

[6] S. Wibowo, S.B. Sumitro, S. Widyarti, Computational study of Cu^{2+}, Fe^{2+}, Fe^{3+}, Mn^{2+} and Mn^{3+} binding sites identification on HSA 4K2C, IOP Conf. Ser. Mater. Sci. Eng. (2020), 833012052.

[7] K. Nagumo, M. Tanaka, V.T.G. Chuang, H. Setoyama, H. Watanabe, N. Yamada, K. Kubota, M. Tanaka, K. Matsushita, A. Yoshida, H. Jinnouchi, M. Anraku, D. Kadowaki, Y. Ishima, Y. Sasaki, M. Otagiri, T. Maruyama, Cys34-Cysteinylated human serum albumin is a sensitive plasma marker in oxidative stress-related chronic diseases, PloS One 9 (1) (2014), e85216.

[8] M. Anraku, V.T.G. Chuang, T. Maruyama, M. Otagiri, Redox properties of serum albumin, Biochim. Biophys. Acta 1830 (12) (2013) 5465–5472.

[9] S. Wibowo, S. Widyarti, A. Sabarudin, D.W. Soeatmadji, S.B. Sumitro, The role of astaxanthin compared with metformin in preventing glycated human serum albumin from possible unfolding: a molecular dynamic study, Asian J. Pharmaceut. Clin. Res. 12 (9) (2019) 276–282.

[10] A. Phaniendra, D.B. Jestadi, L. Periyasamy, Free radicals: properties, sources, targets, and their implication in various diseases, Indian J. Clin. Biochem. 30 (1) (2015) 11–26.

[11] M. Valko, D. Leibfritz, J. Moncol, M.T. Cronin, M. Mazur, J. Telser, Free radicals and antioxidants in normal physiological functions and human disease, Int. J. Biochem. Cell Biol. 39 (2007) 44–84.

[12] B. Grimmig, S.H. Kim, K. Nash, P.C. Bickford, R.D. Shytle, Neuroprotective mechanisms of astaxanthin: a potential therapeutic role in preserving cognitive function in age and neurodegeneration, Geroscience 39 (1) (2017) 19–32.
[13] L. Ekpe, K. Inaku, V. Ekpe, Antioxidant effects of astaxanthin in various diseases-A review, J. Mol. Pathophysiol. 7 (2018) 1–6.
[14] J. Zhang, Z. Sun, P. Sun, T. Chena, F. Chen, Microalgal carotenoids: beneficial effects and potential in human health, Food Funct 5 (2014) 413–425.
[15] J. Chen, K. Fukuzumi, B. Ip, Cid, A.P. Florence, Metal coordination chemistry in the study of biological pathway and processes: a review, IJPBCS 3 (3) (2014) 36–45.
[16] W. Kohn, A.D. Becke, R.G. Parr, Density functional theory of electronic structure, J. Phys. Chem. 100 (1996) 12974–12980.
[17] P. Hohenberg, W. Kohn, Inhomogeneous electron gas, Phys. Rev. 136 (1964) B864–B871.
[18] W. Kohn, L. Sham, Self-consistent equations including exchange and correlation effects, Phys. Rev. 140 (1965) A1133–A1138.
[19] M.J. Frisch, G.W. Trucks, H.B. Schlegel, G.E. Scuseria, M.A. Robb, J.R. Cheeseman, G. Scalmani, V. Barone, B. Mennucci, G.A. Petersson, H. Nakatsuji, M. Caricato, X. Li, H.P. Hratchian, A.F. Izmaylov, J. Bloino, G. Zheng, J.L. Sonnenberg, M. Hada, M. Ehara, K. Toyota, R. Fukuda, J. Hasegawa, M. Ishida, T. Nakajima, Y. Honda, O. Kitao, H. Nakai, T. Vreven, J.A. Montgomery, J.E. Peralta, F. Ogliaro, M. Bearpark, J.J. Heyd, E. Brothers, K.N. Kudin, V.N. Staroverov, R. Kobayashi, J. Normand, K. Raghavachari, A. Rendell, J.C. Burant, S.S. Iyengar, J. Tomasi, M. Cossi, N. Rega, J.M. Millam, M. Klene, J.E. Knox, J.B. Cross, V. Bakken, C. Adamo, J. Jaramillo, R. Gomperts, R.E. Stratmann, O. Yazyev, A.J. Austin, R. Cammi, C. Pomelli, J.W. Ochterski, R.L. Martin, K. Morokuma, V.G. Zakrzewski, G.A. Voth, P. Salvador, J.J. Dannenberg, S. Dapprich, A.D. Daniels, O. Farkas, J.B. Foresman, J.V. Ortiz, J. Cioslowski, D.J. Fox, Gaussian 09, Revision A.02, Gaussian, Inc., Wallingford. CT. USA, 2009.
[20] P.J. Hay, W.R. Wadt, Ab initio effective core potentials for molecular calculations. Potentials for the transition metal atoms Sc to Hg, J. Chem. Phys. 82 (1985) 270–283.
[21] P.J. Hay, W.R. Wadt, Ab initio effective core potentials for molecular calculations. Potentials for K to Au including the outermost core orbitals, J. Chem. Phys. 82 (1985) 299–310.
[22] W.R. Wadt, P.J. Hay, Ab initio effective core potentials for molecular calculations. Potentials for main group elements Na to Bi, J. Chem. Phys. 82 (1985) 284–298.
[23] T.H. Dunning Jr., P.J. Hay, in: H.F. Schaefer III (Ed.), Modern Theoretical Chemistry, Vol. 3, Plenum, New York, USA, 1977.
[24] A.D. Becke, Density-functional exchange-energy approximation with correct asymptotic behavior, Phys. Rev. A. 38 (1988) 3098–3100.
[25] B. Mielich, A. Savin, H. Stoll, H. Peuss, Results obtained with the correlation energy density functionals of becke and lee, yang and parr, Chem. Phys. Lett. 157 (1989) 200–206.
[26] C. Lee, W. Yang, R.G. Parr, Development of the colle-salvetti correlation-energy formula into a functional of the electron density, Phys. Rev. B 37 (1988) 785–789.
[27] M.T. Cances, B. Mennucci, J.A. Tomasi, New integral equation formalism for the polarizable continuum model: theoretical background and applications to isotropic and anisotropic dielectrics, J. Chem. Phys. 107 (1997) 3032–3037.
[28] B. Mennucci, J. Tomasi, Continuum solvation models: a new approach to the problem of solute's charge distribution and cavity boundaries, J. Chem. Phys. 106 (1997) 5151–5158.
[29] N.U. Zhanpeisov, W.S. Ju, M. Anpo, Local structure of highly dispersed lead containing zeolite. An ab initio and density functional theory study, J. Mol. Struct. 592 (2002) 155–160.
[30] Y. Wang, J. Ma, S. Inagaki, Theoretical design of singlet localized sigma-diradicals: $C(Mh_2)_3c$ (M = Si, Ge, Sn, Pb), Tetrahedron Lett. 46 (2005) 5567–5577.
[31] S. Kaenkaew, O. Sae-Khow, V. Ruangpornvisuti, Cation recognition of thiacalix[2] thianthrene and p-tert-butylthiacalix[2]thianthrene and their conformers and complexes with Zn(II), Cd(II) and Hg(II): a theoretical investigation, J. Mol. Model. 16 (2010) 243–253.
[32] F. Kandemirli, B. Köksoy, T. Arslan, S. Sagdınc, H. Berber, Synthesis and theoretical study of bis(fluoroisatinato)mercury(II), J. Mol. Struct. 921 (2009) 172–177.
[33] E. Krieger, G. Vriend, Yasara view - molecular graphics for all devices – from smartphones to workstations, Bioinformatics 30 (2014) 2981–2982.
[34] J.P. Yuan, J. Peng, K. Yin, J.H. Wang, Potential health-promoting effects of astaxanthin: a high-value carotenoid mostly from microalgae, Mol. Nutr. Food Res. 55 (2011) 150–165.
[35] R.R. Ambati, S.M. Phang, S. Ravi, R.G. Aswathanarayana, Astaxanthin: sources, extraction, stability, biological activities and its commercial application, Mar. Drugs 12 (2014) 128–152.
[36] X. Liu, T. Osawa, Cis astaxanthin and especially 9-cis astaxanthin exhibits A higher antioxidant activity in vitro compared to the all-trans isomer, Biochem. Biophys. Res. Commun. 357 (1) (2007) 187–193.
[37] C. Yang, L. Zhang, H. Zhang, Q. Sun, R. Liu, J. Li, L. Wu, R. Tsao, Rapid and efficient conversion of all-E-astaxanthin to 9 Z- and 13 Z-isomers and assessment of their stability and antioxidant activities, J. Agric. Food Chem. 65 (4) (2017) 818–826.
[38] C. Yang, H. Zhang, R. Liu, H. Zhu, L. Zhang, R. Tsao, Bioaccessibility, cellular uptake, and transport of astaxanthin isomers and their antioxidative effects in human intestinal epithelial caco-2 cells, J. Agric. Food Chem. 65 (47) (2017) 10223–10232.
[39] M. Nazifi, M. Asgharshamsi, M. Dehkordi, K. Zborowski, Antioxidant properties of aloe vera components: a DFT theoretical evaluation, Free Radic. Res. 53 (8) (2019) 922–931.
[40] E. Hernández-Marin, A. Barbosa, A. Martínez, The metal cation chelating capacity of astaxanthin. Does this have any influence on antiradical activity? Molecules 17 (2012) 1039–1054.